

Controlling Radiative Heat Transfer Across the Mold Flux Layer by the Scattering Effect of the Borosilicate Mold Flux System with Metallic Iron



DAE-WOO YOON, JUNG-WOOK CHO, and SEON-HYO KIM

The present study proposes a countermeasure for regulating total heat flux through the mold flux layer by designed mold flux with additive metallic iron particles. The heat flux through the B_2O_3 -CaO-SiO₂-Na₂O-CaF₂-Fe system was investigated using the infrared emitter technique to evaluate total flux density across the mold flux film. Both scanning electron microscope (SEM) and X-ray diffraction analysis were employed in order to identify the morphological and compositional changes of the crystalline phase, according to increasing iron contents in the mold flux. It was confirmed that the crystalline layer of studied mold fluxes does not have a meaningful effect on the total heat flux density due to the similar structure and fraction of the crystalline phase. The extinction coefficient was measured for glassy mold fluxes using an ultraviolet/visible and a Fourier transformation-infrared ray spectrometer in the range of 0.5 to 5 μm . For analyzing the scattering behavior of iron particles on the extinction coefficient, the number density and diameter of particles were observed by an automated SEM (auto-SEM). With these data, Mie scattering theory is adopted to define the scattering behavior of dispersed iron droplets in glassy matrix. It was found that the theoretical scattering coefficient demonstrated about 1623 to 3295 m^{-1} , which is in accordance with the experimental results. In doing so, this study successfully achieves the strong scattering behavior that would contribute greatly to the optimization of overall heat flux through the mold flux film during the casting process.

DOI: 10.1007/s11663-017-0975-z

© The Minerals, Metals & Materials Society and ASM International 2017

I. INTRODUCTION

MUCH research has been carried out to understand the thermal behavior through the mold flux between the solidifying shell and copper mold, as the surface quality of slabs is intensively affected by the heat flux during the casting process. It has been acknowledged that surface defects, *i.e.*, longitudinal crack or breakout, on the slab could easily occur by uneven solidification of the steel shell.^[1–3] In order to prevent the nonhomogeneity growth of the solidifying shell and cracks, it is essential to control the heat flux by using the thermal properties of mold flux systems. The liquid-phase mold flux is fed between the steel shell and solidified mold flux film, which has direct contact with the copper mold. Also, the solid flux film is considered to be a mixture of precipitated crystalline layer and glassy phase, where the fraction of each is different depending on the chemical composition of the mold flux and cooling rate.

Each flux layer influences the overall heat flux from the steel shell to the copper mold by means of thermal resistance, which comprises both conduction and radiation. The detailed heat-transfer phenomenon through each mold flux film is described elsewhere.^[4–6]

Many research groups have investigated the heat-transfer phenomenon across the mold flux film by controlling several variables such as the crystallinity degree of flux and additive transition metal oxides within the mold slags.^[5,7–10] Among them, the crystallization of the mold flux with high basicity is well known to be an effective method for reducing the overall heat-transfer rate by a larger interfacial thermal resistance and a low transmissivity of radiation.^[5,7,8] However, highly basic mold fluxes might cause various surface defects such as sticker breakout and streak mark on the slab surface.^[11] Therefore, it is necessary to optimize the thermal properties of the mold flux for better control of both the heat transfer and lubrication in the casting mold. In a previous study,^[12] it was reported that the mold slag system with fine dispersed metallic particles could be used to regulate the heat flux across the mold flux layer thanks to the particle's scattering effects. However, it has not been fully comprehended yet how the scattering effects change the heat flux in the actual continuous casting condition. Hence, it is desirable to investigate systematically the effect of tiny metallic particles on the thermal properties of the mold flux. Therefore, the aim of this study is to

DAE-WOO YOON and SEON-HYO KIM are with the Department of Materials Science and Engineering, Pohang University of Science and Technology (POSTECH), Pohang 37673, Republic of Korea. JUNG-WOOK CHO is with the Graduate Institute of Ferrous Technology, Pohang University of Science and Technology (POSTECH), Pohang 37673, Republic of Korea. Contact e-mail: jungwook@postech.ac.kr

Manuscript submitted September 4, 2016.

Article published online April 18, 2017.

design mold fluxes for reducing the heat flux without negative effects on lubrication of the mold flux layer.

According to previous research,^[7,13,14] measuring the heat flux through the mold flux film could have been successfully done using an infrared emitter technique (IET). Based on its contributions in this study, the modified IET system with better control of one-dimensional heat transfer was used to evaluate the overall heat flux through the mold flux film. By using the IET, CaO-SiO₂-Na₂O-B₂O₃-CaF₂-based mold fluxes with different numbers of metallic particles were tested in order to clarify the effect of the scattering behavior on the total heat flux density during the commercial continuous casting process. The size, morphology, and distribution of particles in the mold flux system were investigated using an automated scanning electron microscope (auto-SEM) equipped with energy-dispersive X-ray spectroscopy (EDS). The crystalline phase of the mold fluxes was identified by X-ray diffraction (XRD). In addition, for a comprehensive understanding of thermal radiation through the glassy flux layer, extinction coefficients were determined using Fourier transformation-infrared ray (FT-IR) and ultraviolet/visible (UV/Vis) spectroscopy with a wavelength of 0.5 to 5.0 μm , which presents the range of irradiated heat energy from the solidifying steel shell. Especially, a contribution of metallic particles on the scattering behavior was discussed based on the Mie scattering theory.

II. EXPERIMENTAL PROCEDURE

A. Sample Preparation

Four mold fluxes based on the sodium borosilicate slag system were examined with different contents of metallic iron particles under 3 μm in diameter. Mold fluxes were melted in a graphite crucible using a muffle furnace at 1673 K (1400 °C) for 300 seconds to homogenize the chemical composition. Then they were quenched in a cylindrical copper mold at room temperature to achieve a fully glassy phase and annealed at 698 K (425 °C) for 1 hour to remove thermal stress. No crystallization was observed after annealing for all samples. The glassy samples were polished into a disk shape of 40 mm in diameter and 4.8 mm in thickness using silicon carbide paper to achieve constant surface roughness and thickness. The polished glassy samples with different numbers of metallic particles were placed individually on the top of the copper mold in the IET for heat-transfer experiments. Meanwhile, the solidified glassy samples were also cut and machined into thin discs for measuring extinction coefficients. The chemical compositions of the mold fluxes are listed in Table I.

B. Heat-Transfer Simulating System

The investigation of the heat flux through the mold flux was carried out using an IET, which is schematically shown in Figure 1. This experimental device is composed of a power controller; command and control

system; and infrared heat source, which is able to emit a radiative heat energy of 1.4 MW/m² at 220 voltages. The emitted light from the heater consists of a wavelength from 0.5 to 6 μm , which is similar to the spectrum of emitting energy from the steel shell in the continuous casting system. Hence, the mold flux film would be exposed to the thermal circumstance close to the industrial continuous casting mold. The radiative heat is focused on the surface of the mold covered by the disk type of glassy mold sample, as shown in Figure 2. The heat flux across the flux disk was determined by the temperature gradient measured with K-type subsurface thermocouples. The thermocouples were placed at 3, 7, 11, and 15 mm below the top surface of the copper mold and are designated as T₁, T₂, T₃, and T₄, respectively. The cooling water inlet and outlet temperature were also marked as T_{in} and T_{out}. Simultaneously, a video recording was carried out to monitor the morphological change by melting, solidification, and crystallization of the mold fluxes. The heating process during the IET experiments is shown in Figure 3, where the incident temperature profile of the heat energy increased to 1.2 MW/m² for 600 seconds and was maintained for 1200 seconds. The subsurface temperature profile of the bare copper mold without sample is shown in Figure 4. Before determining the heat flux through the copper mold, it is assumed that heat flows one dimensionally from the top surface to the subsurface of the mold in a steady state. Subsequently, the heat flux based on Fourier's first law is calculated by measuring the interior temperature gradient between thermocouples:

$$q_x = -k \frac{dT}{dx}, \quad [1]$$

where q_x is the heat flux in the x -direction, dx is the distance between thermocouples, k is the thermal conductivity of copper, and dT is the temperature gradient. The calculated heat flux profile of the bare copper mold is shown in Figure 5.

C. Particle Analysis and XRD Identification

For comprehensive understanding of the scattering behavior, various characteristics of the particles in the sample, such as composition, morphology, and size, were analyzed by an auto-SEM (JSM6980LV, JEOL*).

*JEOL is a trademark of Japan Electron Optics Ltd., Tokyo.

To clarify the particle distribution, the machined glassy samples were etched by 3 vol pct of hydrofluoric acid containing ethanol. After that, the etched samples were cleaned by deionized water in an ultrasonic cleaner to eliminate the contamination on samples. The particle analysis was done for the area of $25.0 \times 10^{-6} \text{ m}^2$ using an SEM with EDS (Oxford) at 15 kV. The backscattered electron mode was applied to identify the particle image. Feature sizing was set up as follows: magnification 250 times, 0.247- μm pixel size, and 4×4 -pixel minimum size corresponding to a lower limit of

Table I. Chemical Composition of Mold Fluxes (Mass Percent)

Sample	SiO ₂	CaO	MgO	Al ₂ O ₃	Fe ₂ O ₃	Na ₂ O	F	B ₂ O ₃	Fe	Basicity (CaO/SiO ₂)
A	33.7	33.8	0.9	4.4	0.1	6.4	6	14.8	0	1.0
B	32.4	32.3	0.9	4.2	0.1	6.1	5.8	14.2	0.5	1.0
C	31.0	31.1	0.8	4.1	0.1	5.9	5.5	13.6	0.8	1.0
D	30.3	30.4	0.8	4.0	0.1	5.8	5.4	13.3	1.0	1.0

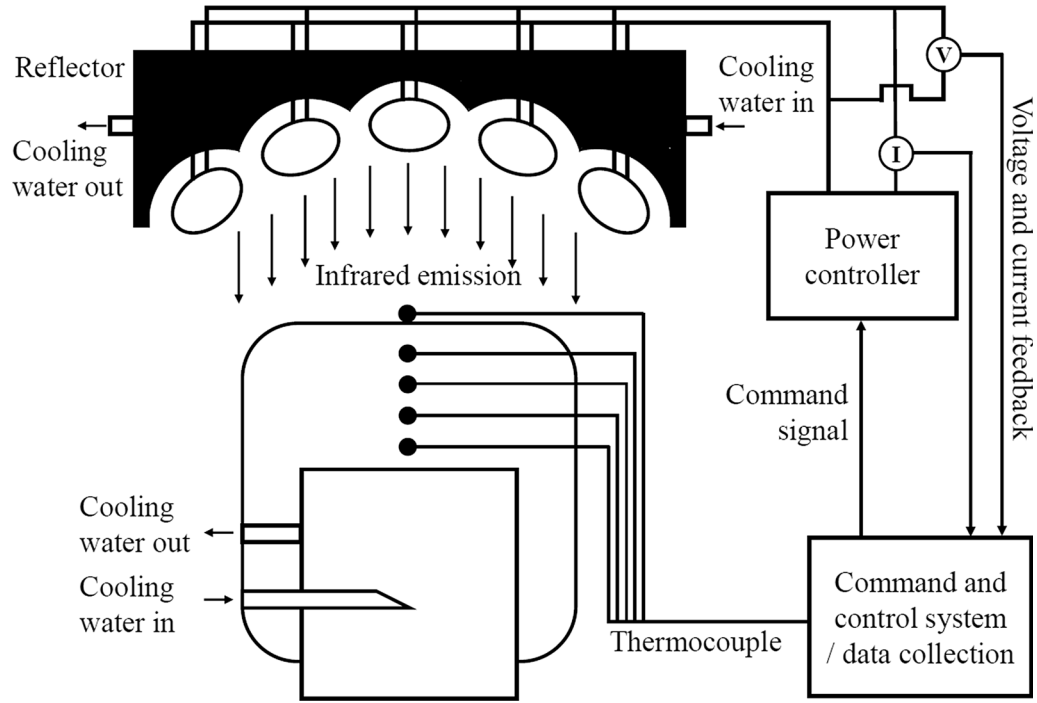


Fig. 1—Schematic of infrared emitter technique.

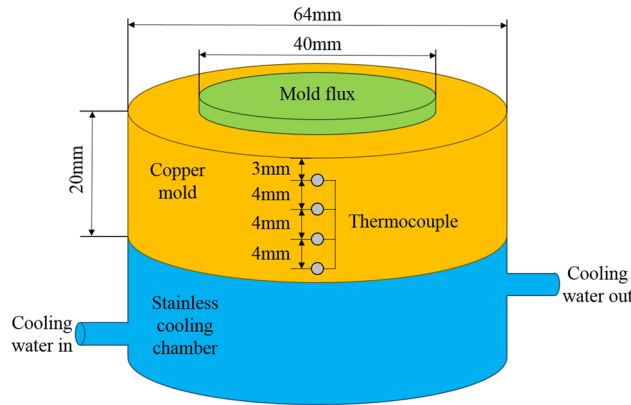


Fig. 2—Schematic of copper mold and target sample.

$0.5 \times 10^{-6} \text{ m}^2$. The residual spectra of the matrix were analyzed for Ca, Si, Mg, Al, Na, Fe, B, and O. To verify the crystalline phase after the IET experiment, all of the samples were ground and sent for XRD analysis. XRD patterns were achieved by an X-ray diffractometer (AXS D8 Advance; Bruker, Germany) with a graphite monochromator using Cu K_α radiation and a scanning rate of 2 deg/min.

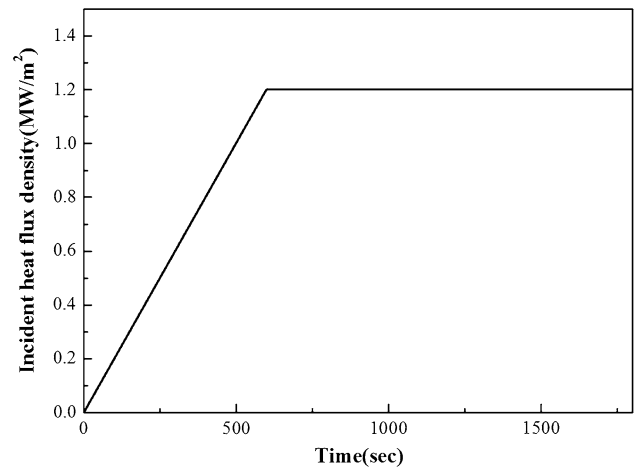


Fig. 3—Heating process of IET experiment.

D. Determining Extinction Coefficients

The extinction coefficient of the glassy mold flux discs was measured with FT-IR (Vertex 80v; Bruker, Germany) and UV/Vis spectrometry (Lambda 750S; PerkinElmer,

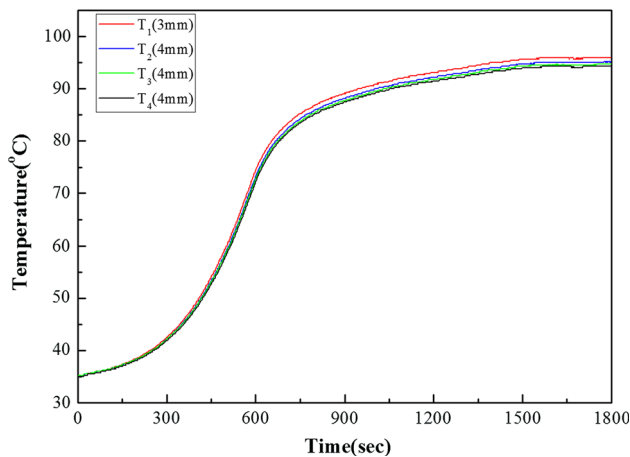


Fig. 4—Responding temperature in mold without glass disk.

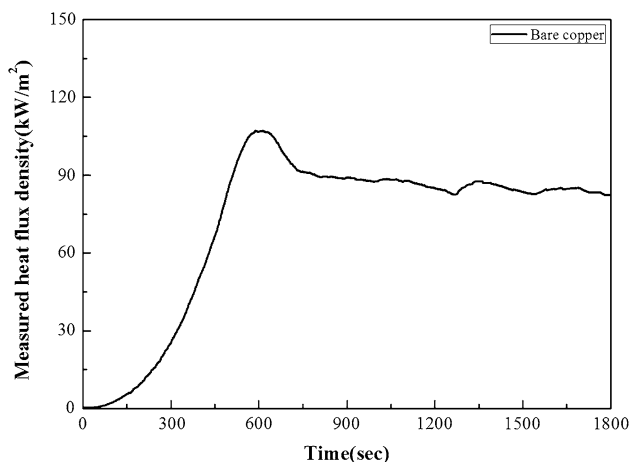


Fig. 5—Measured heat flux profile of bare copper mold.

USA) between 0.5 and 5.0 μm . When incident radiative energy impinges the sample, the beam intensity decreases due to the interaction with the sample, which can be explained by the absorption coefficient, α , and scattering coefficient, s . As the reflectivity of glassy flux film is known to be only 1 to 3 pct,^[6] the dissipation of spectral radiation through a medium can be described by Lambert–Beer’s law (Eq. [2]):

$$\frac{I_T}{I_0} = \exp\{-(\alpha + s)d\}, \quad [2]$$

where I_0 is the intensity of incident beam, I_T is a transmitted beam magnitude, and d is the thickness of the sample. The extinction coefficient is simply the sum of the absorption and scattering coefficients. The details of the procedure have been described elsewhere.^[12]

III. RESULTS AND DISCUSSION

A. In-Situ Observation of Thermal Behavior of Mold Fluxes

The temperature profile during the IET experiment could be divided into five stages for all mold fluxes, as

shown in Figures 6(a) through (d). Stage I involves linearly increasing the heat flux by radiative heat energy from the heat source while the mold flux maintains the glassy phase. In stage II, the heat flux continues to increase, but there is a substantial retardation due to the phase transformation from the glassy mold flux to the crystalline. It is believed that the retardation should be caused by the initiated crystallization of the mold flux. The crystallization of the mold flux appears at the top surface of the flux disk and expands toward the bottom side. All of the heat flux profiles in this stage show a little peak at 399 seconds for disc A, 453 seconds for disc B, 430 seconds for disc C, and 450 seconds for disc D (Figure 6). Stage III is influenced by another phase transformation that arises from the melting of the mold flux. The dissolution of the crystalline phases is initiated at the top surface when the disc reaches the melting temperature, which could be confirmed by the fact that the upper edge of the discs changed to round shape by initiation of the melting, as shown in Figure 6. Also, a steep increase of the heat flux is observed in this period, because the partially crystallized mold fluxes formed at the previous stage begin to melt. This leads to a decrease of the overall thermal resistance and, hence, an increase of the total heat flux. Stage IV is quasi-steady state, where the heat flux tends to reduce due to the developed crystallization and melting phase of the mold flux while the constant heating is applied. Stage V is the steady state; when the phase transformation of the disk was completed, the total heat flux was maintained at a constant rate.

B. Effect of Metallic Particles on the Heat-Transfer Rate and Crystallization Behavior

The measured heat flux profiles of each mold flux with final cross-sectional image are shown in Figure 7. By addition of iron particles into the reference mold flux, sample A, the heat flux shows distinct deviations, as can be seen in stage V. The heat fluxes at steady state are approximately 213, 172, 143, and 121 kW/m^2 for mold fluxes A, B, C, and D, respectively. These results indicate that the steady-state heat-transfer rate decreases with the increase in the metallic particle density in the flux system. It is considered that particles in the matrix are closely related to the scattering behavior, which will be discussed in the following sections. According to the observation of the cross-sectional view of each sample after the IET experiment, it is found that the initial glassy phase of all mold fluxes changes to three layers, liquid layer, crystalline phase, and glassy film, which can be seen in Figure 7. The thickness of each layer was measured and is shown in Table II. It can be observed that the liquid-phase thickness of each sample decreases by an increase in the metallic particle, whereas the thickness of the glassy film increases with the number of particles. The thickness of the crystalline phases, which has a decisive role in the control of the heat transfer across the mold flux layer, was slightly reduced with an increase in particle density, but not significantly. Therefore, the difference in the thickness of the crystalline film was not considered to be the main reason for the change

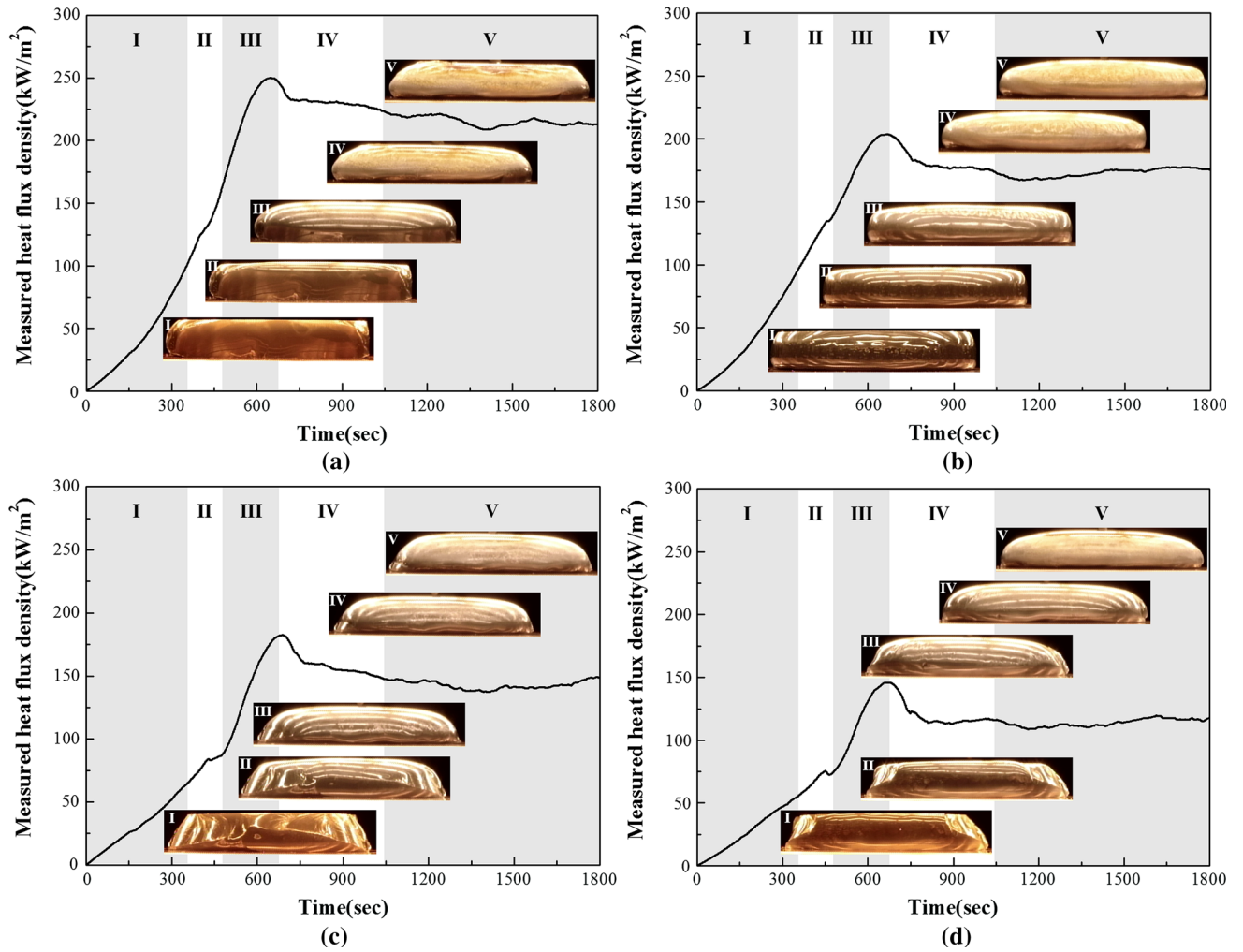


Fig. 6—Measured heat flux profile for (a) sample A, (b) sample B, (c) sample C, and (d) sample D.

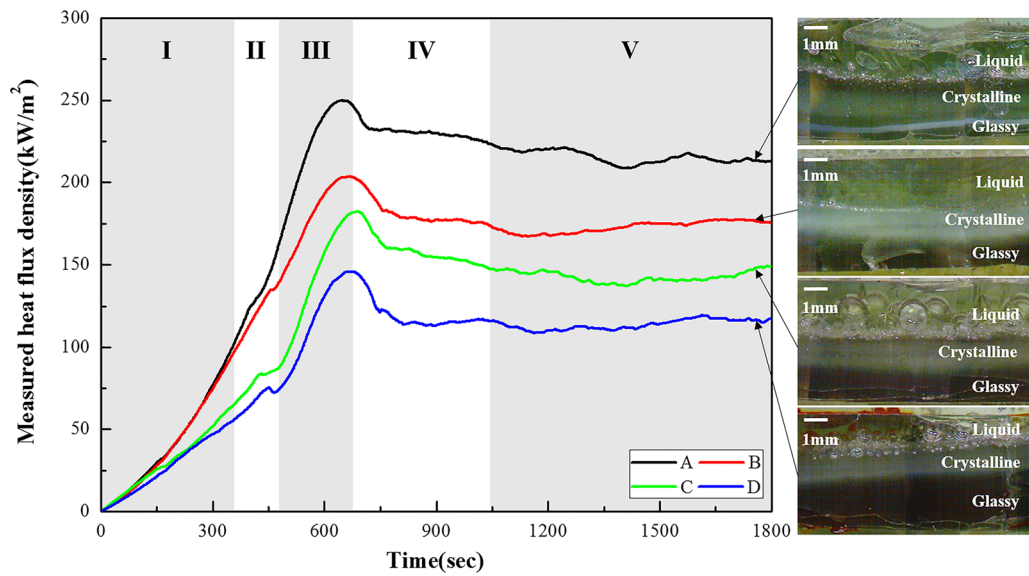


Fig. 7—Comparison of measured heat flux profile for mold fluxes.

of the total heat flux through the mold flux discs. Hence, it is necessary to investigate the distribution, morphology, and fractions of the crystalline layers in more detail.

The results of the SEM analysis for the crystalline phases of A through D mold fluxes after the IET test are shown in Figure 8. The bright spherical droplets were confirmed as metallic iron by SEM-EDS. It can be seen that both the number and size of the spherical metallic particles were increased by increasing the metallic particle concentration. To verify the precipitated phases of the crystalline layer for each mold flux disc, the XRD analysis was conducted for ground powders of all samples. The XRD results of each mold flux are shown in Figure 9. It was confirmed that Cuspidine ($3\text{CaO}_2\text{SiO}_2\text{CaF}_2$) and Wollastonite (CaOSiO_2) are the main compounds corresponding to the peaks of all the mold flux discs. The crystallization of the Cuspidine phase was preceded by the precipitation of acicular Wollastonite crystalline. In Figure 7, only one peak on the heat flux curve can be seen for each mold flux disc in stage II, whereas two crystalline phases of Wollastonite and

Cuspidine were observed from the SEM image in Figure 8. Hence, it is expected that the precipitation of Wollastonite and Cuspidine occurs simultaneously during the crystallization of the mold flux discs. The calcium fluoride (CaF_2) is also identified in the disc sample as having granular structure. The crystalline phases of each sample are largely the same in size and morphology, but it was observed that the fraction of the crystalline shows a relative difference according to each mold flux. In this respect, the degrees of crystallization were calculated and are given in Table III. The results indicate that the crystallinity fraction of the reference mold flux A was lower than that of the iron particles containing mold fluxes. It was previously reported that the surface of particles could serve as the site for heterogeneous nucleation,^[15] which is affected by several parameters such as the particle size, concentration, shape, and other specific interaction characteristics.^[16,17] In Figure 8, it can be seen that metallic particles can behave as the origin for heterogeneous nucleation. Hence, the addition of tiny metallic iron particles into the mold flux could provide effective nucleation sites, which could increase the crystallization of the mold flux. However, increasing the concentrations of metallic particles in the mold flux system would not cause a significant increase of crystallinity degree in this study. D'Haese *et al.* reported that the effect of particles on the nucleation efficiency saturates at lower concentrations near 1 mass pct.^[18] However, the systematic mechanism has not been carried out to understand the saturation particle concentration. Consequently, based on the present results, it is suggested that the existence of

Table II. Thickness of Structural Layers of Mold Fluxes After IET Test (Millimeters)

Sample	A	B	C	D
Liquid	1.92	1.78	1.74	1.48
Crystalline	1.55	1.51	1.51	1.35
Glassy	1.33	1.51	1.55	1.97
Total	4.8	4.8	4.8	4.8

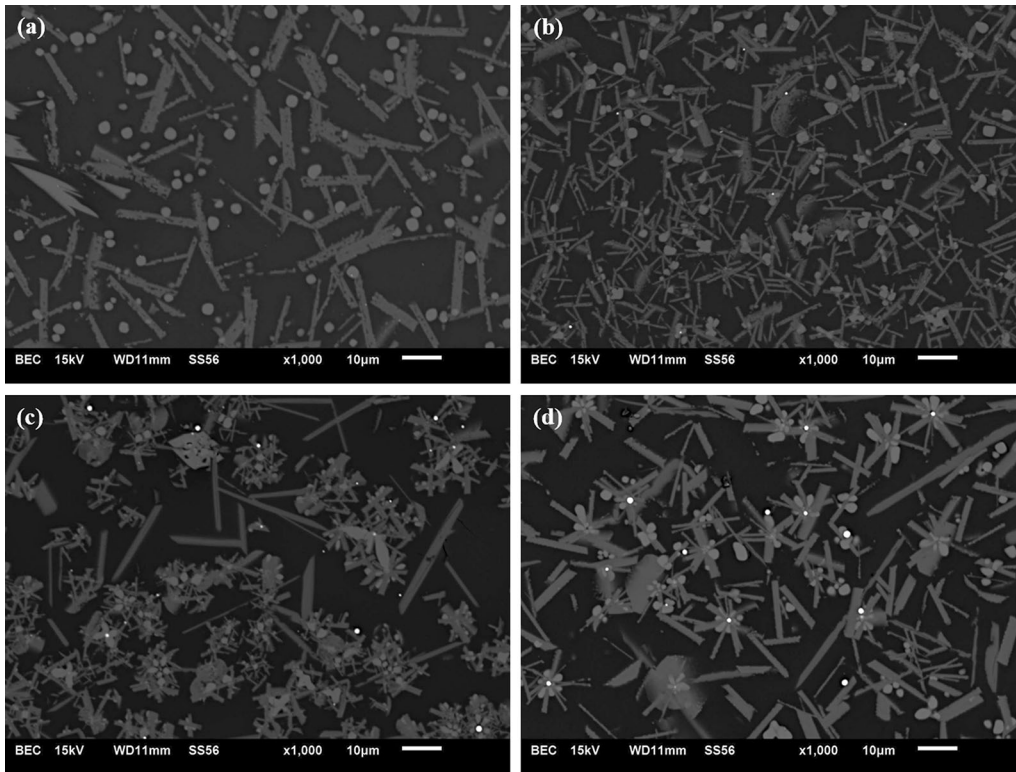


Fig. 8—SEM image of crystalline layer for (a) sample A, (b) sample B, (c) sample C, and (d) sample D.

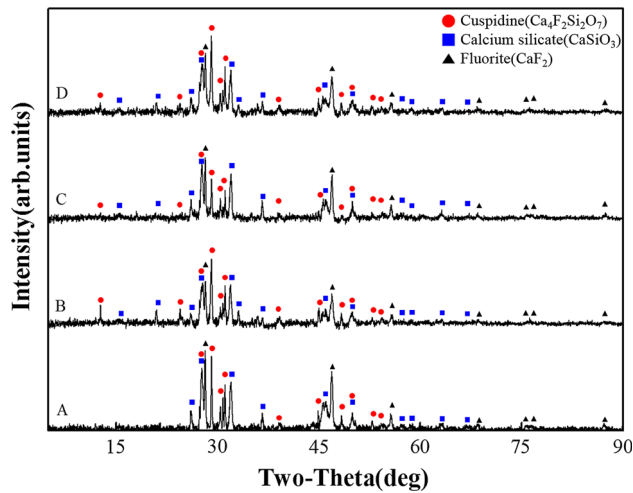


Fig. 9—XRD patterns of mold fluxes for crystalline phases.

Table III. Crystallinity Fraction for Crystalline Phase of Mold Fluxes (Percent)

Sample	Degree of Crystallization (Crystalline Phase/Matrix)
A	25.72
B	38.31
C	35.82
D	31.23

metallic particles in the mold flux would lead to little increase of the crystalline fraction of the mold flux, while the contribution of the crystalline layer to the heat flux would remain largely the same due to similar crystallization characteristics such as crystalline phases and thickness of the crystalline layer regardless of the number of metallic particles. Therefore, it is more likely that the reduced heat-transfer rate would arise from the scattering effect due to the dispersed metallic particles, as discussed in Section III-C.

C. Scattering Effects on Radiative Heat Transfer Through Mold Flux Layer

Radiative heat energy is intensively emitted from the solidifying shell in the range of 1.0 to 5.0 μm on the basis of Planck's law with the assumption of blackbody. Several studies^[8,9,11] have been conducted to clarify the extinction coefficient of mold fluxes in the near infrared range for understanding the radiative heat transfer in the continuous casting mold. The extinction coefficients of all the studied mold fluxes were computed using Eq. [2] based on measured transmissivity. It should be noted that the measurements mentioned previously were performed for the fully glassy disks at lower temperature, which is different from the IET tests. As can be seen in Figure 10, the extinction coefficient of the reference mold flux A is largely below 1000 m^{-1} in the infrared range. The sharp peak of the extinction

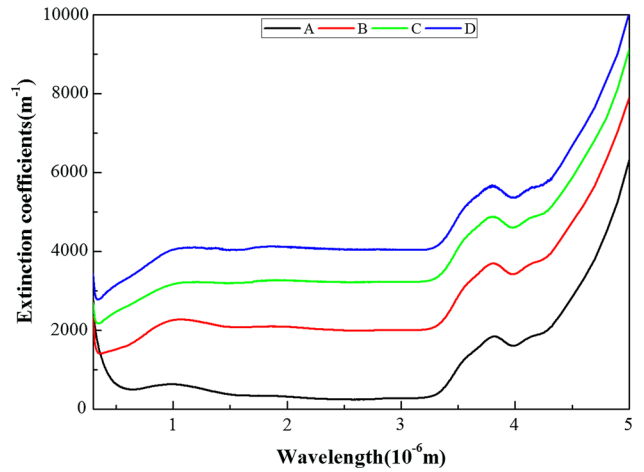


Fig.10—Extinction coefficient of glassy mold fluxes as a function of wavelength.

coefficient for the borate-containing mold fluxes between 3.8 and 4.1 μm is presumed to arise from the ring stretching of the cyclic borate ion,^[19] which would not influence the radiative heat transfer due to the low peak intensity of irradiated energy from the steel shell. On the contrary, the average extinction coefficient of the metallic iron particles containing mold flux shows a drastic increase, for instance, 2450 m^{-1} for mold flux B and 4415 m^{-1} for mold flux D, as shown in Figure 10. This distinct deviation of average extinction coefficients is mainly attributed to scattering factors by different dimensions and the number of particles in the glassy mold flux. Hence, the SEM analysis was applied to investigate the size and number density of the metallic particle for each flux system, as shown in Figure 11. It was observed that numerous spherical particles are dispersed in the glassy matrix, and these fine metallic particles are strongly connected with the extinction coefficient in terms of scattering effects. For evaluating the iron particle distribution, the number density of each mold flux was analyzed in the range above 0.5 μm using an auto-SEM, as shown in Figure 12. It was found that both the number and the size of particles increased with the increasing concentration of tiny metallic irons in the mold flux system. In Figure 13, the particle number densities (A: 0.51, B: 0.81, C: 1.48, and D: 2.1/ 10^{-3}m^{-3}) are well consistent with the average extinction coefficients (A: 733, B: 2450, C: 3618, and D: 4415/ m^{-1}) of glassy discs, while the mean sizes of particles (A: 0.614, B: 1.118, C: 1.102, and D: 1.035/ μm) seem insignificant.

To verify the scattering behaviors by iron particles, the contribution of the scattering factors was extracted from the overall extinction coefficients. As shown in Figures 11 through 13, the reference mold flux A shows a negligible number of particles in the matrix. Therefore, mold flux A is selected as the standard, which makes no scattering contribution to the extinction coefficient. Then the scattering coefficient of other fluxes can be determined by the difference in their extinction coefficients with that of mold flux A, as shown in Figure 14. The mean values of the scattering coefficients from the measured extinction coefficients were approximately

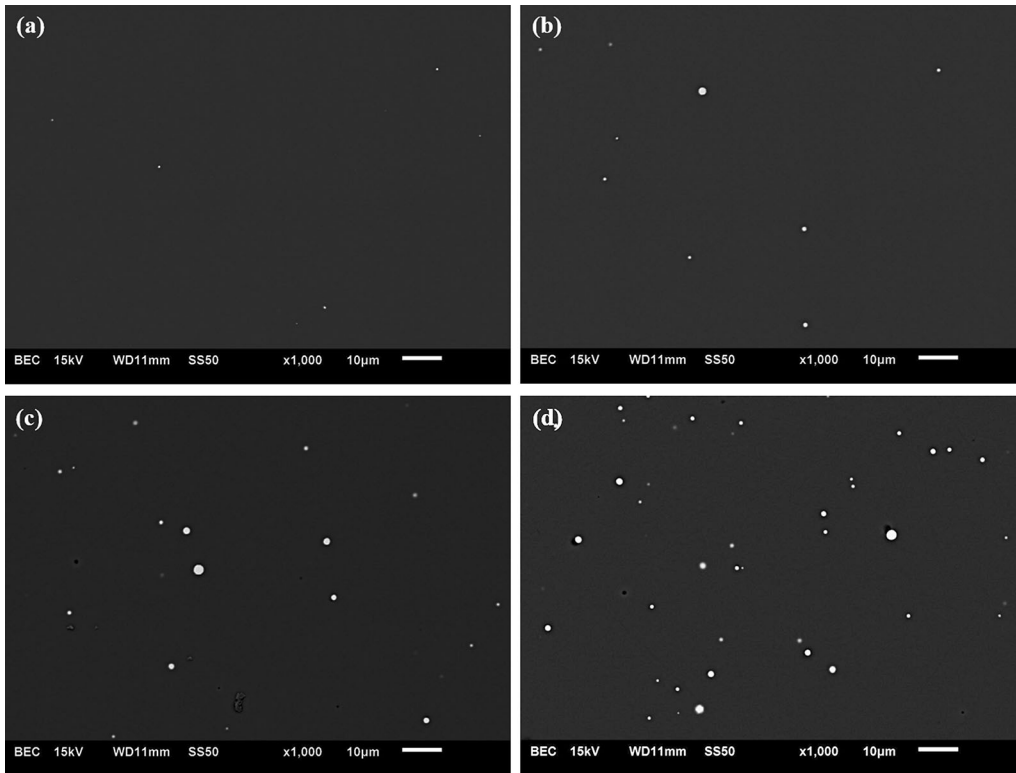


Fig. 11—SEM image of glassy flux disks for (a) sample A, (b) sample B, (c) sample C, and (d) sample D.

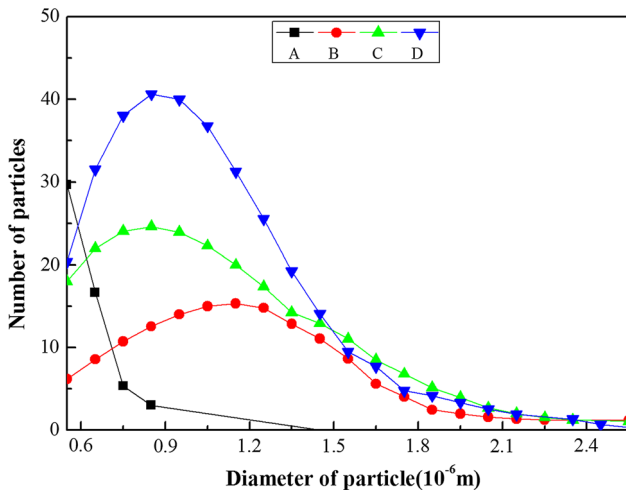


Fig. 12—Number distribution of particles on glassy mold fluxes as a function of diameter.

1717, 2884, and 3682 m^{-1} for glassy mold fluxes B, C, and D, respectively. Samples B through D show considerable scattering behavior because of the fine metallic iron particles in the glassy mold flux. These results agree well with the particle size and distribution shown in Figure 12. Thus, it is necessary to apply the scattering theory for clarification of the scattering phenomenon by spherical particles in the mold flux system. When the photons collide with charged matter, such as electrons and protons, the electric charges should be oscillated due to the secondary emission of

light, which is known to be scattering. Mie scattering theory could well explain the scattering behavior when the scattered frequency by spherical particles is comparable to the incident radiation.^[20] Hence, Mie scattering was applied to evaluate the scattering coefficient through the designed glassy mold flux disc. According to several studies for defining the Mie scattering regime,^[21–23] it has been reported that the centers of scattering geometry are electrically charged spheres and that the plane wave occurs when the electromagnetic field impinges on the homogeneous dielectric sphere. Then the scattering behavior by the spherical particles contained in the flux system can be determined by the refractive index (m), defined as the ratio of iron particles (n_{iron}) and medium particles (n_{med}), and the size parameter (x), which is described by the radius of the particle (r) and the wavelength of the incident light (λ) as $x = 2\pi r/\lambda$. The detailed derivation of the scattering coefficient (μ_s) by Mie theory is described elsewhere.^[12,23] Consequently, the scattering coefficient (μ_s) can be calculated by the following equation:

$$\mu_s = \rho_s \cdot \sigma_s, \quad [3]$$

where ρ_s is the particle number density in the matrix of the unit volume; the numerical values of the scattering cross section (σ_s) were calculated on the basis of the research by Bohren and Huffman.^[24] The data used in the calculation of the scattering coefficients are given in Table IV. For a precise demonstration of the scattering coefficient, the range of size parameters was restricted to below 5 based on several research studies.^[12,28–30] In addition, the refractive index of the

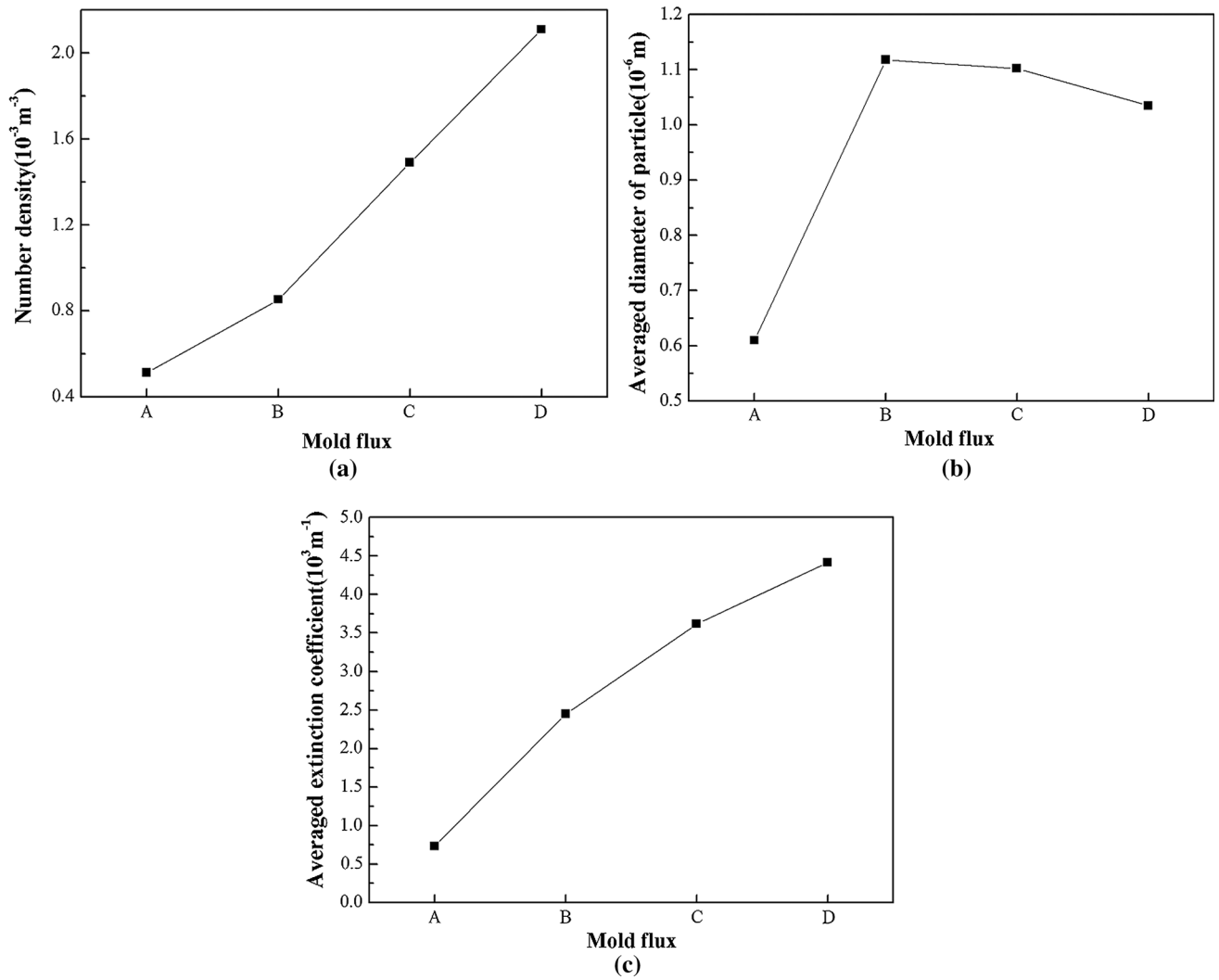


Fig. 13—(a) Number density, (b) averaged diameter of particle, and (c) averaged extinction coefficient of mold fluxes.

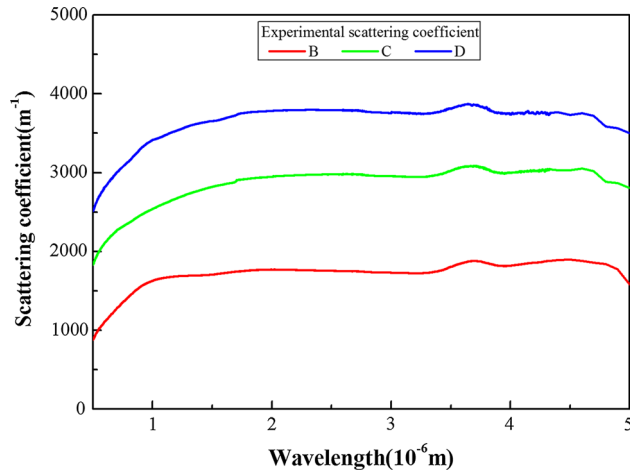


Fig. 14—Experimental scattering coefficients for mold fluxes B through D.

iron particle studied by Johnson and Christy^[25] was applied to reduce the deviation of the real particle and the simulated ones in the wavelength range from 0.5 to

$5 \mu\text{m}$. Then the scattering coefficients were calculated with the modified scattering variables by Eq. [3], as shown in Figure 15. The average values of the theoretical scattering coefficients were nearly 1623, 2558, and 3295 m^{-1} for samples B, C, and D, respectively. It was found that the scattering coefficients by Mie theory are largely coincident with those extracted from the experimental results, where the slight difference arises from the limitation for detecting the size of the particles under $0.5 \mu\text{m}$ during auto-SEM measurement. Therefore, the origin of the increased extinction coefficient with the dispersed metallic particles in the glassy matrix can be logically explained by the Mie scattering theory.

The scattering coefficient is intensively related to the change of the flux through the mold flux layer, as can be seen in Figure 16. In this study, based on the IET experiments, it was confirmed that the total heat flux through the mold flux could be successfully reduced by the scattering effects from numerous spherical particles without the help of the enhanced crystalline phase fraction. Generally, it is widely known that developing

Table IV. Database for Calculating Scattering Coefficients

Wavelength (μm)	Refractive Index			Particle Diameter (μm)	Number Density ($10^{-4}/\text{m}^3$)			
	Iron ($n_{\text{iron}} = n - ik$)*		Medium n_{med} ^[27]		Mold Flux			
	n ^[25,26]	κ ^[25,26]			A	B	C	D
0.5	1.953	2.754	1.6	0.55	3.71	0.98	1.74	2.18
1.0	3.23	4.35		0.65	0.73	0.45	1.84	3.05
				0.75	0.64	0.96	2.64	2.96
1.5	3.572	5.74		0.85	—	0.71	1.69	2.75
				0.95	—	0.63	1.26	2.52
2.0	3.84	7.16		1.05	—	1.14	1.31	2.45
				1.15	—	0.78	0.88	1.25
2.5	4.129	8.59		1.25	—	0.81	0.81	1.44
				1.35	—	0.49	0.62	0.75
3.0	4.359	9.91		1.45	—	0.33	0.49	0.53
				1.55	0.03	0.35	0.54	0.27
3.5	4.483	11.24		1.65	—	0.07	0.32	0.29
				1.75	—	0.1	0.21	0.17
4.0	4.54	12.6		1.85	—	0.09	0.13	0.22
				1.95	—	0.09	0.12	0.03
4.5	4.59	13.96		2.05	—	0.06	0.06	0.11
				2.15	—	0.03	—	0.02
5.0	4.59	15.4		2.25	—	0.02	0.08	—
				2.35	—	—	0.07	0.02
				2.45	—	—	—	0.02

* n is the real part of the refractive index (n_{iron}) and κ is the imaginary index.

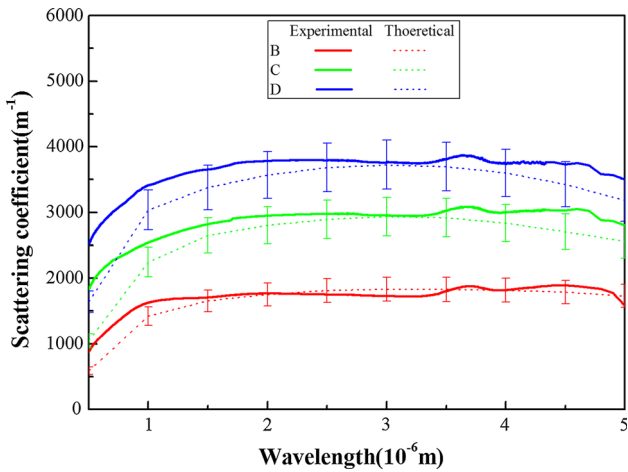


Fig. 15—Scattering coefficients for mold fluxes B through D by Mie theory in comparison with experimental scattering coefficients.

crystallization is useful for decreasing the heat flux density because of the larger reflectivity^[31] or extinction coefficient of the crystalline mold flux. It should be emphasized that the growth of crystallization would induce the detrimental effects on the friction of the steel shell in a casting mold.^[32,33] In this context, it is noteworthy that increases of the scattering coefficient might not result in any negative impact on lubrication. Consequently, the mold flux containing metallic particles of a few microns is appropriate to reduce the total heat flux effectively without promotion of crystallization behavior. The scattering effect of the spherical particles

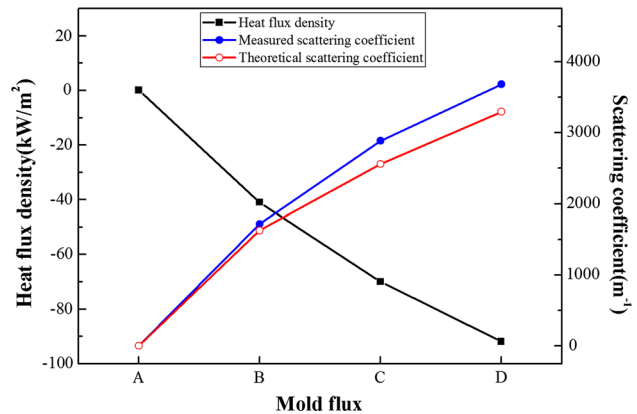


Fig. 16—Change of heat flux and scattering coefficients according to mold fluxes.

closely follows Mie theory, by which the variation of the experimental extinction coefficients could be well reproduced. Hence, it is possible to regulate the total heat-transfer rate across the mold flux layer by using the scattering behavior, which introduces new and advanced techniques for suppression of the surface defects on slabs during the casting process.

IV. CONCLUSIONS

The heat-transfer rate through the mold flux layer was confirmed for $(100 - x)(\text{B}_2\text{O}_3\text{-CaO-SiO}_2\text{-Na}_2\text{O-CaF}_2) + x\text{Fe}$ ($x = 0$ to 1)—based mold fluxes by an

IET simulator. The metallic iron particles and crystalline phase in the matrix were investigated using an SEM and XRD analysis. The extinction coefficients of each glassy mold flux were obtained in the range of 0.5 to 5 μm with measured transmissivity using a FT/IR and UV/Vis spectrometer. In order to verify the scattering effects by the spherical particles, the particle size distribution was analyzed by auto-SEM measurement and defined by Mie scattering theory. The results are summarized as follows.

1. According to the results of the IET experiment, the heat flux at the steady state shows a drastic decreasing trend from 213 to 121 kW/m^2 , corresponding to an increased contribution of iron particles on the mold flux system. It is considered that the particle density on the matrix is strongly associated with the heat-transfer rate in terms of the scattering behavior.
2. The result of the SEM and XRD analysis indicated that the addition of the iron particle into the mold flux system does not have a significant impact on the variation of the thickness for the crystalline mold flux layer or on the structural and compositional changes of the crystalline phase. This investigation showed that the degree of crystallization fluctuated based on the increase of the effective nucleation sites by tiny particles. However, metallic particles over 1 wt pct did not cause further growth of the crystalline fraction because of the saturating nucleation efficiency.
3. The averaged extinction coefficients of the designed glassy mold flux are approximately 733, 2450, 3618, and 4415 m^{-1} , respectively. It is found that the volumetric number densities (A: 0.51, B: 0.81, C: 1.48, and D: $2.1/10^{-3} \text{m}^{-3}$) and averaged particle dimensions (A: 0.614, B: 1.118, C: 1.102, and D: $1.035/\mu\text{m}$) are closely related to the extinction coefficient. This is reasonable due to the fact that the quantity of iron particles in the flux system could highly affect the extinction coefficient in terms of scattering behaviors.
4. To clarify the scattering effect by the spherical particles, Mie theory is applied to confirm the scattering coefficient in the range of 0.5 to 5 μm . Reduced asymmetry values are necessary for the accurate demonstration of scattering effects of the real particles as modifying size parameters. The averaged scattering value by Mie theory is reproduced as about 1623 to 3295 m^{-1} compared to the measured scattering coefficient of 1717 to 3682 m^{-1} . The scattering effects by the metallic particles could be a strong reducing agent of incident radiation, which is capable of controlling heat transfer through the mold flux layer without any fatal side effects on friction during the casting process.

REFERENCES

1. K.C. Mills, A.B. Fox, Z. Li, and R.P. Thackray: *Ironmak. Steelmak.*, 2005, vol. 32, pp. 26–34.
2. J. Konishi, M. Militzer, I.V. Samarasekera, and J.K. Brimacombe: *Metall. Mater. Trans. B*, 2002, vol. 33B, pp. 413–23.
3. M. Hanao, M. Kawamoto, and A. Yamanaka: *ISIJ Int.*, 2012, vol. 52, pp. 1310–19.
4. J.W. Cho, H. Shibata, T. Emi, and M. Suzuki: *ISIJ Int.*, 1998, vol. 38, pp. 268–75.
5. J.W. Cho, T. Emi, H. Shibata, and M. Suzuki: *ISIJ Int.*, 1998, vol. 38, pp. 834–42.
6. J.W. Cho, H. Shibata, T. Emi, and M. Suzuki: *ISIJ Int.*, 1998, vol. 38, pp. 440–46.
7. K. Gu, W. Wang, L. Zhou, F. Ma, and D. Huang: *Metall. Mater. Trans. B*, 2012, vol. 43B, pp. 937–45.
8. C.P. Hallam and W.D. Griffiths: *Metall. Mater. Trans. B*, 2004, vol. 35B, pp. 721–33.
9. J. Diao, B. Xie, J. Xiao, and C. Ji: *ISIJ Int.*, 2009, vol. 49, pp. 1710–14.
10. D.W. Yoon, J.W. Cho, and S.H. Kim: *Met. Mater. Int.*, 2015, vol. 21, pp. 580–87.
11. J.W. Cho, K. Blazek, M. Frazee, H. Yin, J.H. Park, and S.W. Moon: *ISIJ Int.*, 2013, vol. 53, pp. 62–70.
12. D.W. Yoon, J.W. Cho, and S.H. Kim: *Metall. Mater. Trans. B*, 2016, vol. 47B, pp. 2785–92.
13. W. Wang and A.W. Cramb: *ISIJ Int.*, 2005, vol. 45, pp. 1864–70.
14. W. Wang, K. Blazek, and A.W. Cramb: *Metall. Mater. Trans. B*, 2008, vol. 39B, pp. 66–74.
15. B. Wunderlich: *Macromolecular Physics*, vol. 2, *Crystal Nucleation, Growth, Annealing*, Academic Press, New York, NY, 1976, pp. K11–K12.
16. B. Pukanszky: *Eur. Polym. J.*, 2005, vol. 41, pp. 645–62.
17. M. Gahleitner, C. Grein, S. Kheirandish, and J. Wolfschwenger: *Int. Polym. Proc.*, 2011, vol. 26, pp. 2–20.
18. M. D'Haese, F. Langouche, and P.V. Puyvelde: *Macromolecules*, 2013, vol. 46, pp. 3425–34.
19. I.C. Hisatsune and N.H. Suarez: *Inorg. Chem.*, 1964, vol. 3, pp. 168–74.
20. G. Mie: *Ann. Phys.*, 1908, vol. 25, pp. 377–445.
21. S. Asano and G. Yamamoto: *Appl. Opt.*, 1975, vol. 14, pp. 29–49.
22. S. Asano: *Appl. Opt.*, 1979, vol. 18, pp. 712–23.
23. H. Xu, X. Chen, S. Ouyang, T. Kako, and J. Ye: *J. Phys. Chem. C*, 2012, vol. 116, pp. 3833–39.
24. C.F. Bohren and D.R. Huffman: *Absorption and Scattering of Light by Small Particles*, Wiley, New York, 1983, pp. 82–129.
25. P.B. Johnson and R.W. Christy: *Phys. Rev. B*, 1974, vol. 9, pp. 5056–70.
26. M.A. Ordal, R.J. Bell, R.W. Alexander, L.A. Newquist, and M.R. Querry: *Appl. Opt.*, 1988, vol. 27, pp. 1203–09.
27. M. Hayashi, M. Susa, T. Oki, and K. Nagata: *ISIJ Int.*, 1997, vol. 37, pp. 126–33.
28. S. Asano and M. Sato: *Appl. Opt.*, 1980, vol. 19, pp. 962–74.
29. A. Mugnai and W.J. Wiscombe: *Appl. Opt.*, 1986, vol. 25, pp. 1235–44.
30. M.I. Cabrera, O.M. Alfano, and A.E. Cassano: *J. Phys. Chem.*, 1996, vol. 100, pp. 20043–50.
31. M. Susa, A. Kushimoto, R. Endo, and Y. Kobayashi: *ISIJ Int.*, 2011, vol. 51, pp. 1587–96.
32. T. Chikano, K. Ichikawa, and O. Nomura: *Shinagawa Tech. Rep.*, 1988, vol. 31, p. 75.
33. H. Matsuda, K. Saruhashi, J. Abu, H. Takada, H. Yasunaka, and S. Koyama: *CAMP-ISIJ*, 1992, vol. 5, p. 207.